Inverse Hall-Petch Behavior for Nanocrystalline Aluminum Using Molecular Dynamics

Estudio del comportamiento inverso de Hall-Petch en aluminio nanocristalino usando dinámica molecular

Alexandre M. Barboza [1], Luis C. R. Aliaga [2], and Ivan N. Bastos [3]

ABSTRACT

This work investigates the mechanical behavior of nanocrystalline aluminum, with special focus on deformation mechanisms, using molecular dynamics simulations with an interatomic potential parameterized by the authors. To this end, four nanocrystalline samples with grain sizes ranging from 8,2 to 14,2 nm were constructed, each with a volume of 15 x 15 x 20 nm^3. As expected, the data from the tensile tests at a strain rate of 1,0 x 10^9 s^{-1} showed an inverse Hall-Petch relationship. The work hardening behavior revealed no significant gain in mechanical strength. The dislocation analysis indicated that perfect dislocation density decreases during tensile testing, while the Shockley partials increase. Grain boundary-mediated plasticity was evidenced with atomic diffusion along grain boundaries, as well as by grain rotation. Thus, it is concluded that the conventional plastic deformation mechanisms of metals are not preponderant for nanocrystalline aluminum.

Keywords: molecular dynamics, Hall-Petch, mechanical behavior, nanocrystalline aluminum

ABSTRACT

En este trabajo se evalúa el comportamiento mecánico del aluminio nanocristalino, con especial atención a los mecanismos de deformación, utilizando simulaciones de dinámica molecular mediante un potencial interatómico parametrizado por los autores. Para este fin, se construyeron cuatro muestras nanocristalinas con tamaños de grano que oscilaban entre 8,2 y 14,2 nm, cada una con un volumen de 15 x 15 x 20 nm^3. Como se esperaba, los datos de los ensayos de tracción con tasa de deformación de 1,0 x 10^9 s^{-1} mostraron una clara relación inversa de Hall-Petch. El comportamiento de endurecimiento por trabajo mecánico no reveló una ganancia significativa de resistencia mecánica. El análisis de las dislocaciones indicó que las dislocaciones perfectas disminuyen durante los ensayos de tracción, mientras que los parciales de Shockley aumentan. Se evidenció la plasticidad del material con la difusión atómica a lo largo de los límites de grano, así como por la rotación de los granos. De este modo, se concluye que los mecanismos convencionales de deformación plástica de los metales convencionales no son preponderantes para el aluminio nanocristalino.

Palabras clave: dinámica molecular, Hall-Petch, comportamiento mecánico, aluminio nanocristalino

Introduction

Nanocrystalline (NC) metallic materials are a particular case of polycrystalline materials, as their grain size is smaller than 100 nm (Naik and Walley, 2020). These grains have a well-defined atomic arrangement (*i.e.*, body-centered cubic, face-centered cubic, *etc.*) and a large volume fraction of grain boundaries (GBs), which are places of major atomic disorder (Pande and Cooper, 2009). Nanocrystalline materials exhibit interesting mechanical characteristics for various types of applications, as they have, for instance, higher mechanical strength when compared to crystalline alloys of the same chemical composition containing larger grains (Hasan *et al.*, 2020). The relationship between grain size and mechanical strength is given by the Hall-Petch (HP) equation, which can be expressed as follows (Schneider and Laplanche, 2021):

$$\sigma_y = \sigma_0 + k_l d_{GB}^{-1/2} \tag{1}$$

where σ_y is the yield stress, σ_0 and k_l are constants that dependent on the material, and d_{GB} is the average grain size.

The physical explanation of the HP relationship is based on the pile-up model (Baracaldo *et al.*, 2011). Dislocations can usually slip inside a crystal if enough stress is provided and accumulate (pile-up) at some obstacles such as GBs, impurity atoms, second phase precipitates, or other dislocations (Meyers *et al.*, 2006). While the obstacles anchor the dislocations, the plastic deformation is prevented from progressing. However, for every accumulated dislocation, more stress is concentrated at the tip of the pile-up. At some point, the accumulated stress will be such that the obstacle will no longer hold the dislocation pile-up. Consequently, the dislocations will overtake the

[1] Mechanical engineer, Universidade do Estado do Rio de Janeiro (UERJ), Brazil. PhD in Computational Modelling, UERJ, Brazil. Affiliation: Researcher, UERJ, Brazil. E-mail: abarboza@iprj.uerj.br

[2] Bachelor of Physics, Universidad Nacional de Trujillo, Peru. MSc in Physics, Universidade Federal de São Carlos (UFSCAR), Brazil. PhD in Materials Science and Engineering, UFSCAR, Brazil. Affiliation: Professor, UERJ, Brazil. E-mail: aliaga@iprj.uerj.br

[3] Metallurgical engineer, Universidade Federal do Rio de Janeiro (UFRJ), Brazil. MSc in Metallurgical and Materials Engineering, UFRJ, Brazil. PhD in Metallurgical and Materials Engineering, UFRJ, Brazil. Affiliation: Professor, UERJ, Brazil. E-mail: inbastos@iprj.uerj.br

obstacles, continuing with plastic deformation on adjacent grains. Considering the pile-up model, Equation (1), and the fact that NC materials possess an extremely high-volume fraction of GBs, it is clear that they will present enhanced mechanical strength compared to conventional materials.

The HP relationship was believed to be valid for smaller and smaller grains, thus yielding increasingly resistant materials. However, when technology allowed grains to be refined to sizes below a few dozens of nanometers, it was made clear that this relationship was no longer valid. Several studies reported that the yield stress deviates from the HP relationship below a critical grain size, or that even an inverse (or negative) HP relationship is observed (Naik and Walley, 2020; Hu *et al.*, 2017). Figure 1 shows the schematic representation of both regimes: for large grains (conventional HP) and nanograins (inverse HP). The mechanisms by which the inverse HP relationship occurs are not yet well understood.
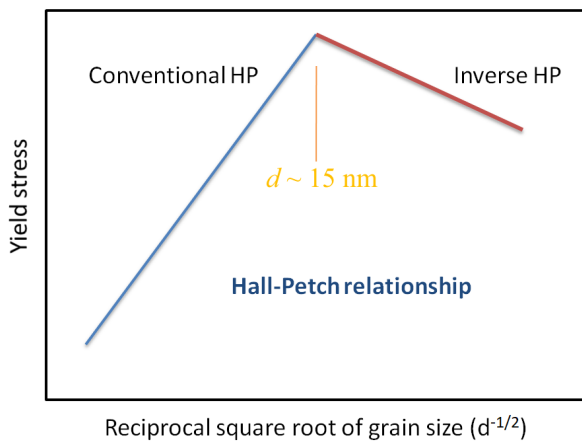

Figure 1. Schematic representation of yield stress dependence on grain size
Source: Authors

The difficulty in manufacturing experimental flaw-free NC samples associated with the progress of computational technology has created an excellent opportunity to study this class of materials by means of computational materials science. By definition, computational materials science involves the computer-based tools employed in modeling and simulation to better understand and predict a material's behavior (Lesar, 2013). It can be used to study alloys (Barboza *et al.*, 2020), glass-forming ability (Aliaga, Lima, *et al.*, 2019; Aliaga, Schimidt, *et al.*, 2018), ceramics and polymers (Tjong, 2013), biocomposites (Kashan and Ali, 2019), and many more systems. Furthermore, computational materials science allows studying phenomena and properties that would be too complex to be tested experimentally due to high pressures/temperatures, deformation rates, heating/cooling rates, or any other physical variable that exceeds the technological capability for actual execution. A computational method often used to study NC materials' behavior is molecular dynamics (MD) simulations.

Molecular dynamics is a simulation method used to study the motion of atoms and molecules by applying classical mechanics (Afkham *et al.*, 2017). The force acting on an atom i, in a system composed of N atoms, can be described as follows (Lee, 2012; Tschopp *et al.*, 2008):

$$\vec{F}_i = m_i \vec{a}_I = m_i \frac{d\vec{v}_i}{dt} = m_i \frac{d^2 \vec{r}_i}{dt^2} = -\frac{dU(\vec{r}_N)}{d\vec{r}_i} \qquad (2)$$

where m_i, $\vec{a}_i$, $\vec{v}_i$, $\vec{r}_i$, and $U(\vec{r}_N)$ are the atomic mass, acceleration vector, velocity vector, position vector, and interatomic potential, respectively. It can be seen in Equation (2) that the force acting on an atom can be obtained from the interatomic potential, which is a function of the position of all atoms. In theory, it would be enough to integrate Equation (2) in order to obtain the velocity and position. However, this results in the classical physical N-body problem, which does not have an analytical solution. Thus, MD simulations employ numerical methods such as the velocity Verlet algorithm (Pal and Ray, 2020).

To reduce the computational cost, the MD considers the atom as a rigid sphere, neglecting the interaction of electrons (Lee, 2012). This technique drastically reduces the complexity of the simulation and thereby its runtime. There is, however, a negative consequence: the interatomic potentials need to be empirically generated, either by fitting certain functions with experimental information or with calculated data from first-principles methods (Lee, 2012). In general, a simulation using MD can be summarized in the following steps:

- Given the initial positions, velocities, and interatomic potential of the atoms, the interaction forces are calculated.

- With the force information, positions are advanced in time by a small interval called *timestep*, which results in new positions, velocities, and forces.

- This new information is then used as input for a new iteration, repeating the previous steps until an equilibrium state is reached.

Various data are stored for each timestep, such as energy, atomic positions, forces, pressure, and temperature. The stored values vary according to the need of each study. The properties that can be calculated with these data are diverse: coefficient of expansion, melting point, thermal conductivity, mechanical/structural properties, among others.

Compared to other methods, such as the first-principles, MD is faster and can handle larger systems. However, one significant disadvantage is its spatial and temporal scale, which is limited to the *nano* range. Moreover, information regarding magnetic properties can not be obtained.

The essence of an MD simulation lies in the interatomic potential, which informs how the forces acting on each atom are calculated. Although there are several interatomic potentials available in the literature for Al, this study used an Embedded Atom Method (EAM) potential parameterized by ourselves via the RAMPAGE technique (Ward *et al.*, 2012). In fact, this potential was initially created to study an Al-Ti-Ni alloy (Barboza *et al.*, 2020). Regarding pure Al, the used potential is capable of reproduce its lattice constant, elastic constants, and cohesive energy. More details regarding the parameterization methodology can be seen in Barboza *et al.* (2020). The key idea of the EAM potential is based on the principle that the system's total energy results from the contribution of the pair potential energy between atoms (the

result of interaction forces), and a term that depends on the local density at the point where each atom is located (Jang et al., 2021). Therefore, by using the EAM formalism, the atom's energy, U_i, can be represented as follows (Saidi *et al.*, 2017):

$$U_i = \frac{1}{2} \sum_{j \neq i} \phi_{ij}(r_{ij}) + F_i(\mu_i) \quad \text{(3a)}$$

$$\mu_i = \sum_{j \neq i} f_i(r_{ij}) \quad \text{(3b)}$$

where $\phi_{ij}(r_{ij})$ is the interaction function of atomic pairs, $F_i(\mu_i)$ is the energy of embedded atoms concerning the electronic density μ_i, r_{ij} is the scalar distance between two atoms i and j, and $f_i(r_{ij})$ is the partial contribution of electronic densities.

It is important to note that, while computational tools are of great value, one should investigate the differences between simulation and experimental results. Experiments that would take hundreds of thousands of seconds are modeled in a few nanoseconds. This discrepancy may exclude some time-dependent phenomena, thus leading to erroneous results. For this reason, it is essential to evaluate the effectiveness of a given computational tool, comparing it with known phenomena obtained from real tests whenever possible.

Nanocrystalline Al has been extensively studied via computational approaches, such as the recent work by Xu and Dávila (2017). However, the vast majority of these works vary the number of atoms and, consequently, the volume of the samples in order to reduce the computational cost, which may negative impact the results.

In this context, this work investigates the mechanical behavior and mechanisms responsible for the plasticity of NC Al by molecular dynamics using all samples with the same volume and number of atoms. Thus, the parameter that varies in our case is the number of grains in each sample. In addition, the interatomic potential used is another novel approach, as it has never been applied to study this metal.

Methodology

The simulations were performed using the Large Scale Atomic/Molecular Massively Parallel Simulator (LAMMPS) code (Plimpton, 1995). As the name suggests, LAMMPS is based on the concept of parallel computing to optimize the processing power. In addition to processors, it also has implementation packages that allow the Graphics Processing Unit (GPU) to run in parallel with the processors, increasing the processing power; this work made use of the GPU package. The NC aluminum samples were initially generated from different seeds with random locations and crystallography directions using a region of $15 \times 15 \times 20$ nm^3 and 271 708 atoms by means of the Atomsk software (Hirel, 2015). In total, four NC samples with different quantities of grains were generated. The average grain sizes were 14,2, 11,9, 9,4, and 8,2 nm for samples with 3, 5, 10, and 15 grains, respectively. The samples were initially relaxed at 300 K, maintaining the external pressure in all directions at 0 Pa with periodic boundary conditions. Subsequently, the samples were loaded into LAMMPS for

the uniaxial tensile test performed at a strain rate of 1,0 x 10^9 s^{-1} along the z-axis.

After the tensile test, the 10- and 15-grain samples were chosen to perform a work hardening study, as they have the smallest average grain size and, therefore, the grain boundary effect is enhanced. The work hardening study was performed by loading the samples to a deformation level of 0,06 (beyond the elastic deformation), unloading, and loading one last time. The work hardening was performed under the same temperature and strain rate used in the tensile test.

Results and discussion

Grain morphology in the considered volume is shown in Figure 2, and the distribution of grain volumes for each NC sample is depicted in Figure 3. Since the total volume of the samples is constant (4 500 nm^3), the histogram shows that samples with fewer grains occupy a larger individual grain volume.
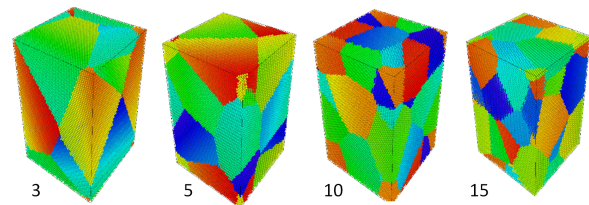

Figure 2. Depiction of Al NC samples. From left to right: samples with 3, 5, 10, and 15 nanograins. The colors are to aid the identification of the grains.
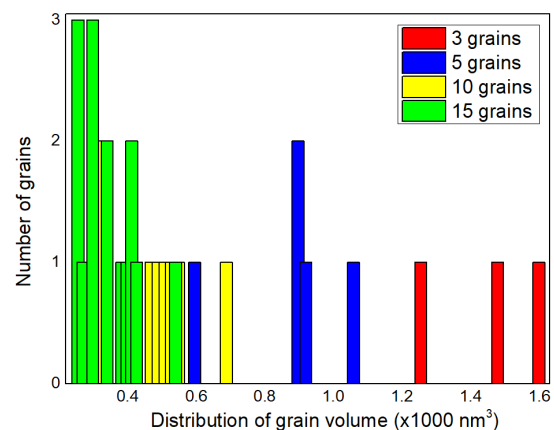**Source:** Authors

Figure 3. Grain volume distribution of the NC samples
Source: Authors

Figure 4 shows the three-grain sample before and after the tensile test. An increase in length along the z-axis and a relatively small decrease in x- and y-directions are observed, as is expected in this type of test. Plastic deformation occurs homogeneously without variation in the total volume.

The simulated stress-strain curves are shown in Figure 5. For all generated nanocrystals, the grain sizes are much smaller than 100 nm. Thus, the inverse HP behavior is expected. The sample with 15 grains (smallest grain size) shows the lowest mechanical resistance. In contrast, the sample with three grains (largest grain size) exhibits the highest strength, with the five- and ten-grain samples presenting intermediate
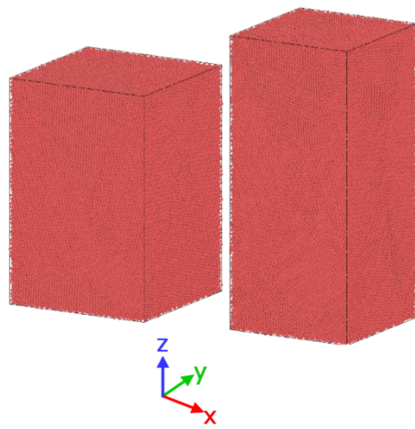
Figure 4. The three-grain NC sample before (left) and after (right) uniaxial tensile testing
Source: Authors

Figure 6. Tensile strength versus the reciprocal square root of the grain size: black squares and green circles represent experimental values reported in literature, whereas red triangles denote simulated results found in this work. The blue and red dashed lines are the linear fit of the corresponding HP behaviors.
Source: Authors

stress values and obeying the inverse HP relationship. It is important to note that the mechanical strength of NC Al is higher when compared to conventional coarse-grained systems, in agreement with other studies (Xu and Dávila, 2017).
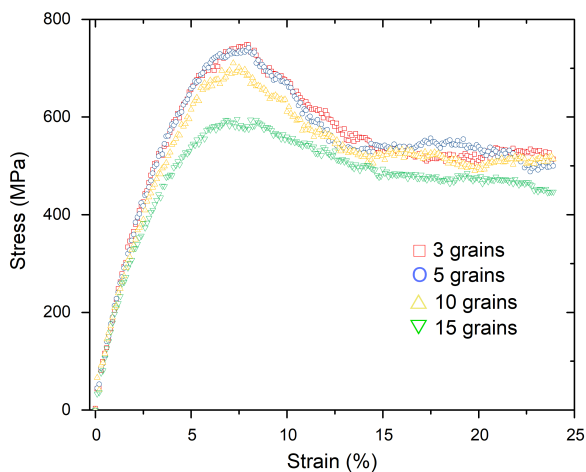

Figure 5. Stress-strain curves of nanocrystalline samples
Source: Authors

The similar mechanical behavior between the three- and five-grain samples is because they are close to the transition from a conventional to an inverse HP relationship. This transition does not occur abruptly; a parabolic trend is expected, as computationally reported for Cu (Weng and Barai, 2009), and experimentally for 0,6%C steel (Baracaldo et al., 2011). Thus, for materials with grain sizes close to the parabola vertex, the difference between their stress values is small compared to materials with grain sizes far from the vertex. For this reason, the difference between the stress values for the five- and ten-grain samples was not pronounced.

Experimental tensile testing of samples with grain sizes ranging from micrometer to nanometer for Al with at least 99% purity can be found elsewhere (Tsuji et al., 2002; Choi et al., 2009). Figure 6 presents the combination of these data with the results of this MD work. The ultimate tensile strength was used in Figure 6 instead of yield stress in order to ease the visualization of HP regimes.
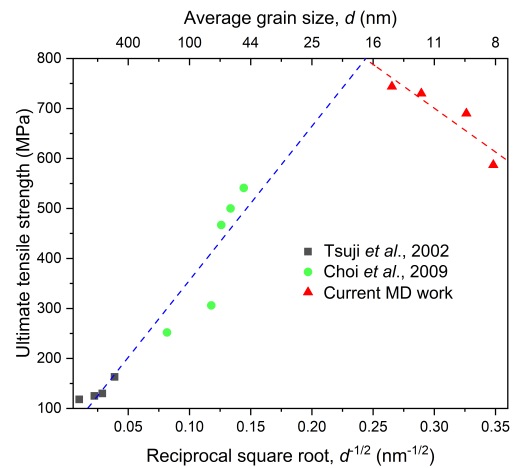
The pattern in Figure 6 resembles the expected behavior of the schematic representation of Figure 1. Moreover, the fitted intersection corresponds to a grain size of approximately 17 nm. Even though it is within the expected grain size transition value from conventional to inverse HP relationship for metals, the 17 nm value might be even smaller in practice. This assumption is based on two reasons: (i) the fitting curves of Figure 6 were extrapolated to cover the full axis range, jeopardizing the results, especially for grain sizes below 50 nm due to the dearth of reliable experimental data; (ii) although it is not shown in Figure 1, a reduction in the conventional HP relationship slope is expected at grain sizes below 100 nm, thus changing its direction. Unfortunately, to reach a grain size of 17 nm, it would be necessary to decrease the number of grains even further, which is impractical in our case, since the sample with largest grain size only has three grains. A decrease in this quantity of grain would place the samples closer to a single crystal than to a polycrystalline structure. Thus, the only way to verify if this grain size value indeed marks an HP regime transition for the NC Al while applying the same methodology of this work would be to reconstruct all samples using larger volumes, which is in intended to be done in future works.

The reasons why the inverse HP relationship occurs are still under debate, but there are indications that the conventional dislocation slip mechanisms are not fully functional at the *nano* scale (Fan et al., 2005; Pande and Cooper, 2009). Instead, GB-mediated mechanisms should dominate the plastic deformation of NC materials (Fan et al., 2005), such as grain boundary sliding and room-temperature Coble creep (Ovid'ko and Shinerman, 2013), i.e., diffusion of atoms along the GBs. To evaluate if the dislocation mechanism persists for NC Al, the work hardening behavior of the 15 and 10-grain samples was investigated. It is well-known that the work hardening phenomenon occurs, basically, by the generation and interaction of the dislocation stress fields. Thus, it is expected that NC samples would not exhibit strain hardening, since the reduced grain sizes would hinder or even inhibit the generation of dislocations. Figure

7 shows the stress-strain curves before and after the work hardening of the 15-grain sample. The 10-grain sample had a similar behavior and was not exhibited.
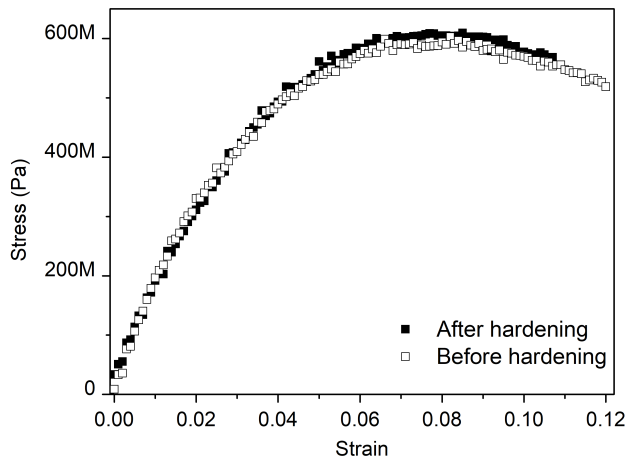

Figure 7. Tensile test after work hardening of the 15-grain sample
Source: Authors

The results reported in Figure 7 confirm the expectation that no significant increase in strength should be observed after strain hardening for NC systems. Therefore, for the conditions applied in this work, dislocations are not responsible for the plastic deformation. However, a diffusion mechanism along GBs (Coble creep) was evidenced, as shown in Figure 8 for the 15-grain sample: grain boundaries are well defined before loading, but after a strain of 0,06, it is possible to observe some atoms migrating along the neighboring grains due to diffusion. Furthermore, the grains are rotated from their original position.
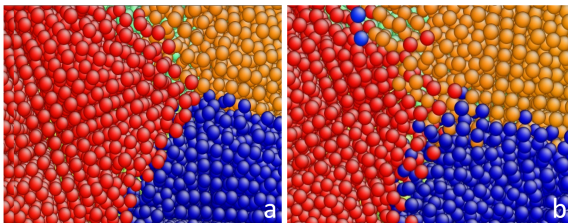

Figure 8. A triple junction in the 15-grain sample: (a) Grain boundaries before the tensile test and (b) after a strain of 0,06. Note the small displacement of atoms along GBs
Source: Authors

To investigate the dislocation dynamics, the dislocation extraction algorithm was used, as implemented in the Ovito software (Stukowski, 2010), which has the function of quantifying the dislocation density for different strains values. Figure 9 shows the dislocation segments for the three-grain sample at strain values of 0,00 and 0,10. Frank and Stair-Rod dislocations are present, but their quantities are negligible in comparison with Shockley partials.

Perfect dislocations are present in a small amounts at the beginning of deformation, and they decrease linearly with the strain. However, Shockley partials grow exponentially, as shown in Figure 10 for the sample with three grains as an example. All the other samples follow this same trend. The parameter ρ is the dislocation density at a given strain, while ρ_0 denotes the initial dislocation density, and the dislocation ratio (normalized dislocation density) is expressed as ρ/ρ_0.
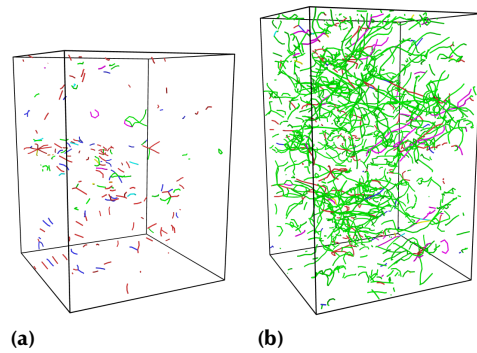

Figure 9. Dislocation evolution of the three-grain sample at strain levels of (a) 0,00 and (b) 0,10. The colors green, strong blue, light blue, purple, and red represent Shockley, perfect, Frank, Stair-Rod, and non-identified dislocations, respectively. Atoms were removed to ease the visualization of the dislocation segments.
Source: Authors

The decreasing of perfect dislocation density is expected, as new perfect dislocations are not possible because of the inhibited Frank-Read source. Moreover, the already existing perfect dislocations are dissociated into two Shockley partials or absorbed by the GBs; both processes reduce its density. The increase in Shockley partials indicates the formation of stacking faults and twinning structures. These results are similar to those obtained for NC Ni (Barboza *et al.*, 2021) and an $Al_{85}Ti_{15}Ni_5$ alloy (Barboza *et al.*, 2020). Finally, the increase in partial dislocations for NC Al was also reported in Xu and Dávila (2017), demonstrating that the interatomic potential applied in this work is capable of reproducing such phenomenon.
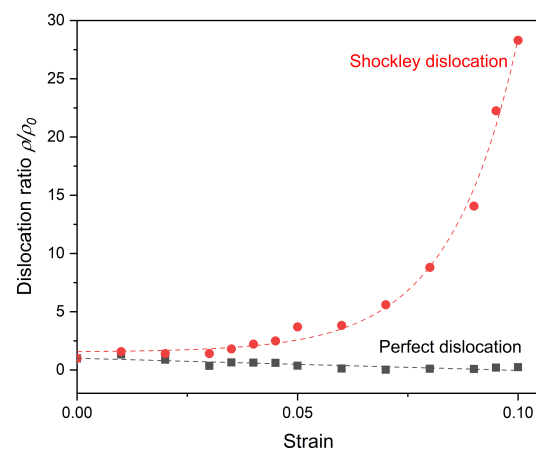

Figure 10. Dislocation ratio (normalized dislocation density) for different strain values of the three-grain sample. The red and black dashed lines are the exponential and linear fit, respectively.
Source: Authors

Conclusions

Molecular dynamics simulations were employed with a novel interatomic potential for Al in order to investigate its mechanical properties and behavior. The tensile testing results clearly showed an inverse Hall-Petch relationship. The grain size transition from the conventional to the inverse Hall-Petch relationship was calculated to be around 17 nm by fitting pertinent data. No work hardening was

observed for the 10- and 15-grain samples. An increase in partial dislocations was observed, but its contribution to the total deformation was limited. For instance, a strain of 0,10 causes a relatively small increase in dislocation density of just one order of magnitude. Coble creep atomic diffusion and grain rotation were evidenced, demonstrating that the conventional slip mechanisms are not predominant for grains in the nanosize. Therefore, further studies are required to better understand these two crucial deformation mechanisms in nanocrystalline materials.

Acknowledgements

References

Afkham, Y., Bahramyan, M., Mousavian, R. T., and Brabazon, D. (2017). Tensile properties of AlCrCoFeCuNi glassy alloys: A molecular dynamics simulation study. *Materials Science and Engineering A, 698*, 143-151. https://doi.org/10.1016/j.msea.2017.05.057

Aliaga, L. C. R., Lima, L. V. P. C., Domingues, G. M. B., Bastos, I. N., and Evangelakis, G. A. (2019). Experimental and molecular dynamics simulation study on the glass formation of CuZrAl alloys. *Materials Research Express, 6*, 045202. https://doi.org/10.1088/2053-1591/aaf97e

Aliaga, L. C. R., Schimidt, C. S., Lima, L. V. P. C., Bastos, I. N., and Botta, W. J. (2018). Study of glass forming on Cu60.0Zr32.5Ti7.5 alloy by molecular dynamics simulation. *Materials Research, 21*(2), e20170555. https://doi.org/10.1590/1980-5373-MR-2017-0555

Baracaldo, R. R., Marrero, J. M. C, and Páramo, A. B. (2011). Studying the Hall-Petch effect regarding sub-micrometer steel (0.6%C). *Ingeniería e Investigación, 31*(3), 112-120. https://doi.org/10.15446/ing.investig.v31n3.26398

Barboza, A. M., Bastos, I. N., and Aliaga, L. C. R. (2020). Molecular dynamics simulations of the mechanical behavior of nanostructured and amorphous $Al_{80}Ti_{15}Ni_5$ alloy. *Revista Facultad de Ingeniería, 103*, 20-33. https://doi.org/10.17533/udea.redin.20201009

Barboza, A. M., Bastos, I. N., and Aliaga, L. C. R. (2021). Nanograin size effects on deformation mechanisms and mechanical properties of nickel: A molecular dynamics study. *Materials Express, 11*(11), 1841-1855. https://doi.org/10.1166/mex.2021.2091

Choi, H. J., Lee, S. W., Park, J. S., and Bae, D. H. (2009). Positive deviation from a Hall-Petch relation in nanocrystalline aluminum. *Materials Transactions, 50*, 640-643. https://doi.org/10.2320/matertrans.MRA2008343

Fan, G.J., Choo, H., Liaw, P. K., and Lavernia, E. J. (2005). A model for the inverse Hall-Petch relation of nanocrystalline materials. *Materials Science and Engineering A, 409*, 243-248. https://doi.org/10.1016/j.msea.2005.06.073

Hasan, M. S., Lee, R., and Xu, W. (2020). Deformation nanomechanics and dislocation quantification at the atomic scale in nanocrystalline magnesium. *Journal of Magnesium and Alloys, 8*, 1296-1303. https://doi.org/10.1016/j.jma.2020.08.014

Hirel, P. (2015). Atomsk: A tool for manipulating and converting atomic data files. *Computer Physics Communications, 197*, 212-219. https://doi.org/10.1016/j.cpc.2015.07.012

Hu, J., Shi, Y. N., Sauvage, X., Sha, G., and Lu, K. (2017). Grain boundary stability governs hardening and softening in extremely fine nanograined metals. *Science, 355*, 1292-1296. https://doi.org/10.1126/science.aal5166

Jang, H.-S., Seol, D., and Lee, B.-J. (2021). Modified embedded-atom method interatomic potentials for Mg-Al-Ca and Mg-Al-Zn ternary systems. *Journal of Magnesium and Alloys, 9*, 317-335. https://doi.org/10.1016/j.jma.2020.09.006

Kashan, J. S., and Ali, S. M. (2019). Modeling and simulation for mechanical behavior of modified biocomposite for scaffold application. *Ingeniería e Investigación, 39*, 63-75. https://doi.org/10.15446/ing.investig.v39n1.73638

Lee, J.G. (2012). *Computational materials science: An introduction*. Taylor & Francis Group.

Lesar, R. (2013). *Introduction to computational materials science — Fundamentals to applications*. Cambridge University Press.

Meyers, M. A., Mishra, A., and Benson, D.J. (2006). Mechanical properties of nanocrystalline materials. *Progress in Materials Science, 51*, 427-556. https://doi.org/10.1016/j.pmatsci.2005.08.003

Naik, S. N. and Walley, S. M. (2020). The Hall-Petch and inverse Hall-Petch relations and the hardness of nanocrystalline metals. *Journal of Materials Science, 55*, 2661-2681. https://doi.org/10.1007/s10853-019-04160-w

Ovid'ko, I. A., and Shinerman, A. G. (2013). Kinects of grain boundary sliding and rotational deformation in nanocrystalline materials. *Reviews on Advanced Materials Science, 35*, 48-58. https://www.ipme.ru/e-journals/RAMS/no_13513/04_13513_ovidko.pdf

Pal, S., and Ray, B. C. (2020). *Molecular dynamics simulation of nanostructured materials: An understanding of mechanical behavior*. CRC Press.

Pande, C. S., and Cooper, K. P. (2009). Nanomechanics of Hall-Petch relationship in nanocrystalline materials. *Progress in Materials Science, 54*, 689-706. https://doi.org/10.1016/j.pmatsci.2009.03.008

Plimpton, S. (1995). Fast parallel algorithms for short-range molecular dynamics. *Journal of Computational Physics, 117*, 1-19. https://doi.org/10.1006/jcph.1995.1039

Saidi, P., Dai, C., Power, T., Yao, Z., and Daymond, M. R. (2017). An embedded atom method interatomic potential for the zirconium-iron system. *Computational Materials Science, 133*, 6-13. https://doi.org/10.1016/j.commatsci.2017.02.028

Schneider, M., and Laplanche, G. (2021). Effects of temperature on mechanical properties and deformation mechanisms of the equiatomic CrFeNi medium-entropy alloy. *Acta Materialia, 204*, 116470. https://doi.org/10.1016/j.actamat.2020.11.012

Stukowski, A. (2010). Visualization and analysis of atomistic simulation data with OVITO - The Open Visualization Tool. *Modelling and Simulation in Materials Science and Engineering, 18*, 015012. https://doi.org/10.1088/0965-0393/18/1/015012

Tjong, S.-C. (2013). *Nanocrystalline materials: Their synthesis-structure-property relationships and applications* (2nd ed.), Elsevier.

Tschopp, M. A., Spearot, D. E., and McDowell., D. L. (2008). Influence of grain boundary structure on dislocation nucleation in FCC metals. *Dislocations in Solids, 14*, 46-139. https://doi.org/10.1016/S1572-4859(07)00002-2

Tsuji, N., Ito, Y., Saito, Y., and Minamino, Y. (2002). Strength and ductility of ultrafine grained aluminum and iron produced by ARB and annealing. *Scripta Materialia, 47*, 893-899. https://doi.org/10.1016/S1359-6462(02)00282-8

Xu, W., and Dávila, L. P. (2017). Tensile nanomechanics and the Hall-Petch effect in nanocrystalline aluminium. *Materials Science & Engineering A, 710*, 413-418. https://doi.org/10.1016/j.msea.2017.10.021

Ward, L., Agrawal, A., Flores, K. M., and Windl, W. (2012). Rapid production of accurate embedded-atom method potentials for metal alloys. *arXiv*. https://doi.org/10.48550/arXiv.1209.0619

Weng, G. J., and Barai, P. (2009). Mechanics of very fine-grained nanocrystalline materials with contributions from grain interior, GB zone, and grain-boundary sliding. *International Journal of Plasticity*, 25, 2410-2434. https://doi.org/10.1016/j.ijplas.2009.04.001